SPE-188472-MS

Evaluation of Viscously Unstable Water Flooding with Gravity Effects and Permeability Heterogeneities Through High-Resolution Simulations

G. Vaillant and R. de Loubens, Total S.A.

This paper was prepared for presentation at the Abu Dhabi International Petroleum Exhibition & Conference held in Abu Dhabi, UAE, 13-16 November 2017.

Abstract

This paper aims at evaluating the interactions between gravity segregation and viscous fingering during water injection into viscous oils, in order to estimate the recovery factor accurately, e.g. before assessment of tertiary EOR mechanisms. Based on simulations of homogeneous and heterogeneous reservoir sector models with horizontal wells, we wish to identify the dimensionless groups affecting the water breakthrough time and the oil recovery, and to quantify the impact of viscous instabilities in 3D domains versus 2D vertical cross-sections.

High-resolution numerical simulations, based on very fine grids and a high-order spatial discretization scheme implemented in our parallel in-house research reservoir simulator, were required to properly capture the complex flow patterns of these two-phase immiscible displacements. We analyze the competition between viscous and gravity effects using different values of injection flow rate, oil viscosity, density difference between oil and water and domain aspect ratio. This analysis is carried out in 2D and 3D, for simple permeability distributions with different correlation lengths, by inspection of production data and saturation maps.

For the investigated range of parameters, capillary effects are negligible and we identify three flow regimes before water breakthrough. When gravity dominates, viscous fingering is strongly attenuated by the rapid formation of a gravity tongue but a 'ridge instability' phenomenon may occur. In contrast, when viscous forces are preponderant, the gravity tongue is very weak or non-existent, and the flow pattern in vertical cross-sections is often characterized by one dominant viscous finger. In the transition regime, the gravity tongue and the viscous fingers coexist and may reach the producer quasi-simultaneously, leading to an optimum injection velocity in terms of breakthrough sweep efficiency. We then examine the dependency of water breakthrough and oil recovery upon the end-point mobility ratio and the viscous-to-gravity ratio $R_{v/g} = \left(\frac{\mu_o U}{k_v \Delta\rho g}\right) \frac{H}{L}$. We also compare the early-time and late-time impacts of permeability heterogeneity and transverse viscous fingering.

In the context of viscous oil recovery by water injection, high-resolution simulations are required to represent the interplay between gravity segregation, viscous fingering and permeability heterogeneity. In the present study, under low capillary effects, it is quite remarkable that the post-breakthrough recovery is well

predicted by 2D simulations and is mostly controlled by two dimensionless groups. This may be useful to create screening models for quick-look estimation of oil recovery on different sector models representative of an oil field.

Introduction

Viscous fingering is a well-known type of instability in porous media flow, which may occur when a less viscous fluid is injected into a more viscous one. Its effects increase with the adverse mobility ratio and the injection velocity. A direct consequence of viscous fingering in the case of unstable water flooding may be a significant bypassing of the resident oil and poor recovery.

Gravity effects on viscous fingering for two miscible fluids have been addressed extensively in the literature. Two-dimensional and three-dimensional simulation results were compared for both homogeneous and heterogeneous porous media, using a mixed finite-difference/particle-tracking approach [1]: it was found that unstable displacements in 3D porous media can be different from displacements in 2D vertical cross-sections, especially in the transition from flow dominated by a single gravity tongue – gravity layer formed along the bottom boundary due to the density contrast – to flow dominated by viscous fingering. In other numerical studies based on a combination of high-order spectral methods and compact finite differences (cf.[2] and [3]), the influence of the density contrast, viscosity ratio, flow rate and aspect ratio on the characteristics of the displacement was investigated quantitatively in rectilinear geometry (using 2D simulations) and in a quarter five-spot geometry (using 3D simulations). The interaction of viscous fingering with gravity segregation was also investigated for heterogeneous reservoirs with different permeability layers [4] and for slightly tilted anisotropic reservoirs [5]: the results of the unstable gas/oil flows dominated by a gravity override were compared with the experiments described in [6]and the onset of viscous fingering was explored.

Immiscible two-phase flows with capillary and gravity effects were studied within homogeneous porous media when the gravity is oriented in the direction parallel to mean flow, e.g.[7],[8],[9]. However, when the mean flow direction is perpendicular to the gravity acceleration, as may occur in oil reservoirs, the interactions between viscous and buoyancy effects in two-phase immiscible displacements have only been partially addressed using high-resolution 2D simulations [10]. The impact of gravity segregation and capillary pressure on the evolution of macroscopic viscous fingers was analyzed in terms of four dimensionless numbers: mobility ratio, capillary number, gravity number and domain aspect ratio. It was found that – for the investigated range of parameters – the viscous fingers can be eliminated even with a small density contrast, resulting in a dominant gravity tongue.

The ultimate recovery factors from viscous oil fields undergoing water flood were gathered and correlated (r^2=0.63) with a function incorporating the volume of water injected, the oil viscosity and the well spacing [11]. While such an approach may be of practical interest for a rough estimation of oil recovery before a field development, there is still a need to identify the most relevant dimensionless numbers in the presence of competing gravity, capillary and viscous effects, so as to improve our quick-look estimation tools. In particular, the relative importance of viscous and gravity effects was already characterized by several dimensionless numbers (e.g. [12], [2], [1],[6]). In this work, we express the viscous-to-gravity ratio $R_{v/g}$ as;

$$R_{v/g} = \left(\frac{\mu_o U}{k_v \Delta\rho g}\right)\frac{H}{L}$$

where U denotes the Darcy velocity, μ_o the oil viscosity, $\Delta\rho$ the density difference between water and oil, g the acceleration due to gravity, k_v the vertica permeability, H the formation thickness, and L the inter-well distance or any macroscopic length of interest. $R_{\_(v/g)}$ can be interpreted as the ratio between two time scales, i.e. $R_{v/g} = \tau_g/\tau_v = \tau_g$where $\tau_g = \phi H/U_z$ is associated with the vertical migration of water through the

reservoir layer of thickness H and porosity ϕ assuming gravity-induced flow at velocity $U_z = K_v \Delta\rho g/\mu_o$, and $\tau_v = \phi L/U$ is associated with the piston-like propagation of a water front from the injector to the producer.

In this paper, we analyze the competition between viscous and gravity effects during viscously unstable water flooding, in both homogeneous and heterogeneous reservoir sector models. Firstly, we describe the main parameters of the reservoir model and the numerical options of our simulations. Secondly, we describe the different flow patterns identified before water breakthrough, by looking at the time evolution of the saturation maps. Thirdly, after checking if 2D vertical simulations can be used to reproduce the 3D early-time results accurately, we determine whether the dimensionless number $R_{v/g}$ and the viscosity ratio $M = \mu_o/\mu_w$ are sufficient to estimate the water breakthrough time; we then study the influence of the main physical and geological parameters on the breakthrough time. Finally, we analyze the relevance of $R_{v/g}$ and M to estimate the oil recovery during the fully-developed regime after water breakthrough, depending on the relative strength of capillary pressure. For this purpose, a large number of 2D simulations were run, after observing on a few representative cases that the 2D and 3D late-time results were very similar.

Methodology

Model description

The main characteristics of the reservoir model used in this paper are based on a large-scale simulation model of a field located in Africa. A sketch of the reservoir sector model geometry, also showing the position of the two horizontal wells, is provided in *Figure 1*.

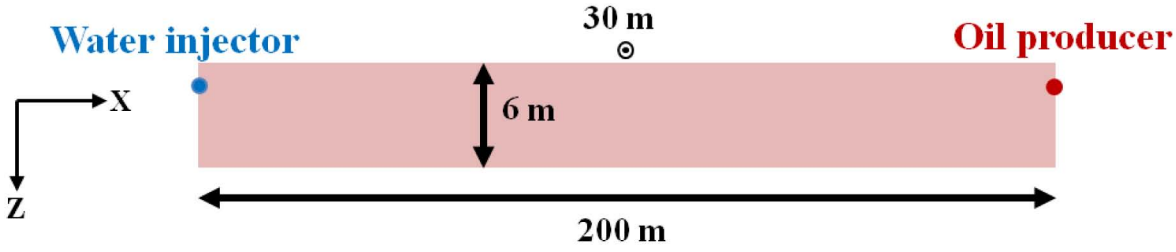

Figure 1—Reservoir sector model geometry

- **Geometry**: In our base case scenario, we consider a three-dimensional 'sugar-box' domain of dimensions 200 m x 30 m x 6 m. Domains of 200 m x 30 m x 3 m and 100 m x 30 m x 6 m will also be considered to investigate the impact of the domain aspect ratio. We verified that a lateral extension of 30 m was much greater than the typical wavelength of transverse viscous fingering, i.e. a larger width has little (if no) impact on the flow pattern and the production profiles. We will also use two-dimensional models based on vertical slices of the 3D models.
- **Grid dimension**: We performed a convergence study under mesh refinement to determine the 3D grid cell sizes required to properly capture the complex flow patterns. The following values were selected: Δx=50 cm, Δy=50 cm and Δz=2.5 cm, leading to 5,76 million cells.
- **Porosity field**: It is considered to be homogeneous with ϕ=0.3.
- **Permeability field**
    - Four horizontal permeability fields are considered: a homogeneous one of 10 Darcy and three heterogeneous ones generated using a lognormal distribution (mean of 10 Darcy, standard deviation of 4 Darcy) and different variograms with a vertical correlation length set to 0.2 m and different horizontal correlation lengths l_{corr} set to 2 m, 5 m and 10 m. Please refer to *Figure 2* for an illustration of those three heterogeneous permeability fields. For 2D simulations, we extract 2D slices of the permeability fields at Y=15m.

- Three values of the vertical-to-horizontal permeability ratio k_v/k_h will be tested: 0.1, 0.3 and 0.9.

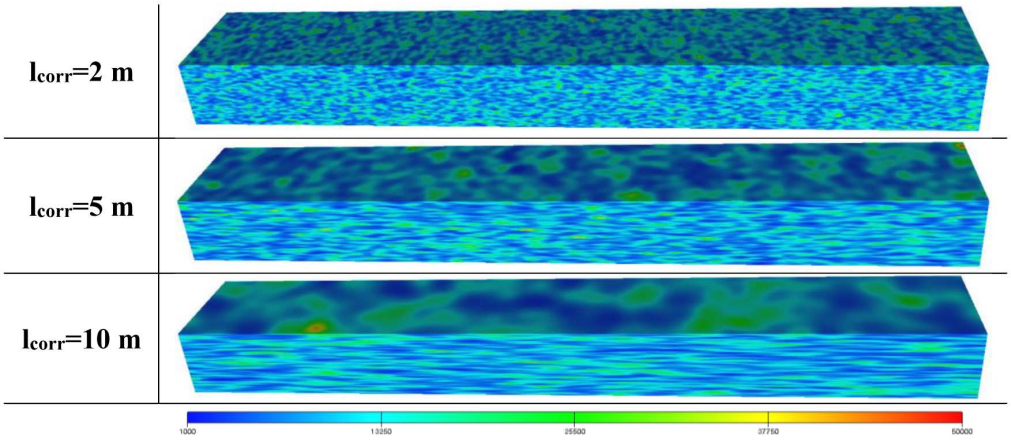

Figure 2—Heterogeneous horizontal permeability fields for various correlation lengths

- **Fluids**: The reservoir contains dead oil and water that are considered as two immiscible and nearly incompressible fluids. Different values of oil density and viscosity are considered for different scenarios, whereas property values for water are fixed:
  - Oil density from 800 to 950 kg/m^3 and water density of 1000 kg/m^3
  - Oil viscosity μ_o from 50 to 200 cP and water viscosity of 0.5 cP
- **Relative permeability curves**: We use Corey-type functions, i.e. $k_{rw} = k_{rw,max}\left(\frac{S_w - S_{wr}}{1 - S_{or} - S_{wr}}\right)^{n_w}$ and $k_{ro} = k_{ro,max}\left(\frac{1 - S_w - S_{or}}{1 - S_{wr} - S_{or}}\right)^{n_o}$ with residual water saturation S_{wr}=0.15, residual oil saturation S_{or}=0.25, maximum oil relative permeability $k_{ro,max}$=1, maximum water relative permeability $k_{rw,max}$=0.4, oil exponent n_o=1.5 and water exponent n_w=3. The resulting curves are represented in *Figure 3 (a)*. The end-points being kept constant, variations of the end-point mobility ratio are only due to variations of the viscosity ratio; our analysis will therefore be based on the viscosity ratio instead of the end-point mobility ratio.
- **Capillary pressure curve**: It is based on the logBeta correlation formulated in [13], with different amplitudes: $p_{c,high}$=5 $p_{c,medium}$ =25 $p_{c,low}$ (cf. *Figure 3 (b)*). For the heterogeneous models, we use the J-function formulation associated to theses curves with a reference permeability of 10 Darcy.

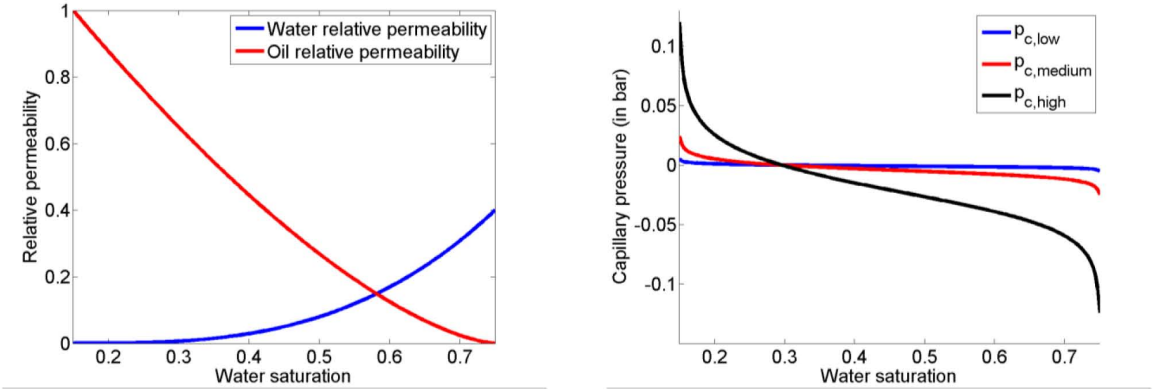

(a) (b)

Figure 3—Oil and water relative permeabilities and (b) capillary pressure curves

- **Reservoir initialization**: Initially, the reservoir pressure is at 50 bars and the water saturation is uniformly equal to S_{wr}.
- **Two horizontal wells**:
  - The water injector is located 1 meter below the reservoir top at X=0 m. It is controlled by a constant flow rate value Q between 2 and 18 m^3/day, depending on the injection scenario. This corresponds to an average Darcy velocity U (based on the whole layer thickness) lying between 1.1 and 10 cm/day. With the maximum injection flow rate, the bottom hole pressure (BHP) reaches a peak of 95 bars.
  - The producer is located 1 meter below the reservoir top at X=200 m, with a BHP target of 50 bars.

We here summarize the parameters that will be varied in the course of this study:

- the oil viscosity: 50, 100 and 200 cP
- the oil density, from 800 to 950 kg/m^3
- the capillary pressure curve: $p_{c,low}$, $p_{c,medium}$ and $p_{c,high}$
- the injection flow rate, from 2 to 18 m^3/day
- the domain dimensions: 200 m x 30 m x 6 m, 200 m x 30 m x 3 m and 100 m x 30 m x 6 m
- the vertical-to-horizontal permeability ratio: 0.1, 0.3 and 0.9
- the permeability field: homogeneous or heterogeneous with different horizontal correlation lengths: 2 m, 5 m and 10 m

Simulation options

The simulations were run using our parallel in-house research reservoir simulator IHRRS (cf. [14],[15]) based on a Darcy-type formulation. In [16], we discussed the validity of Darcy-type models for viscous oils, and showed that for very high viscosity ratio (e.g. > 2000) the multiphase extension of Darcy's law is no longer valid, due to a violation of the continuum and local capillary equilibrium assumptions. However, for the type of viscous oils considered in this work (i.e. below 200 cP) it is reasonable to assume that the generalized Darcy's law is correct enough to represent unstable water floods characterized by macroscopic viscous fingers.

We used a third-order accurate Total Variation Diminishing scheme for the spatial discretization [17] (highly accurate in smooth regions and oscillation-free across discontinuities) and the IMPES time integration scheme (computationally less expensive and numerically less diffusive than the fully implicit method). The time-step size was selected so that it always satisfies the CFL condition (with a safety margin applied to it) and the restriction due to the capillary diffusion term; we verified that the nonlinear solver always converged in 1 or 2 Newton iterations (2 Newton iterations being required only at very early times). The simulations were run on our in-house cluster, using 6 processors in 2D and 384 processors in 3D.

Description of the main flow patterns before water breakthrough

For the investigated range of parameters, capillary effects were negligible and three flow patterns were identified before water breakthrough:

- a 'gravity-dominant' flow regime, with a strong gravity tongue, and possibly some ridge instabilities (*Figure 4* and *Figure 5*)
- a transition flow regime, with a gravity tongue coexisting with macroscopic fingers (*Figure 6*)

- a ‘viscous-dominant’ flow regime, with dominant macroscopic fingers and a quasi non-existent gravity tongue (*Figure 7*)

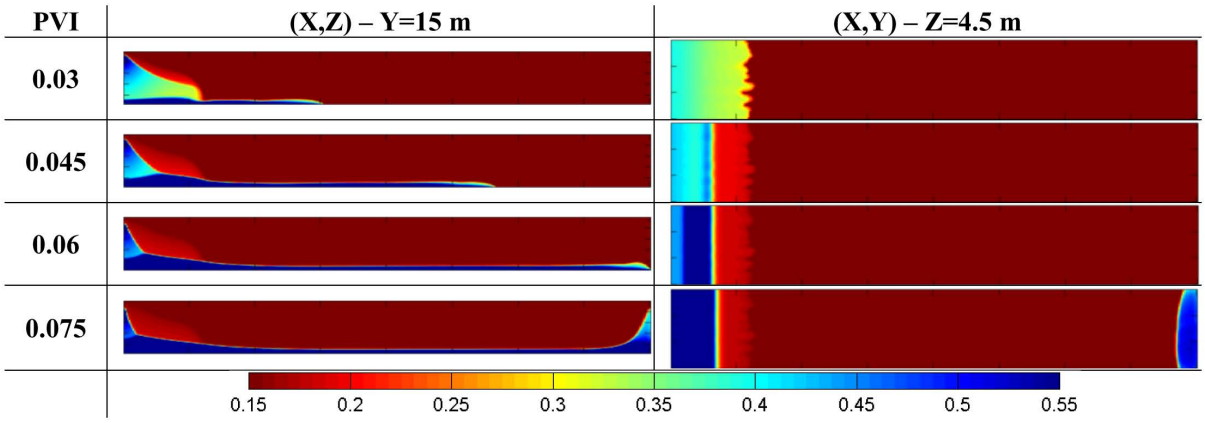

Figure 4—Water saturation in 2D vertical and horizontal cross-sections for a ‘gravity-dominant’ case, without ridge instabilities: Q=4 m³/day, Δρ=200 kg/m³, k_v/k_h=0.3

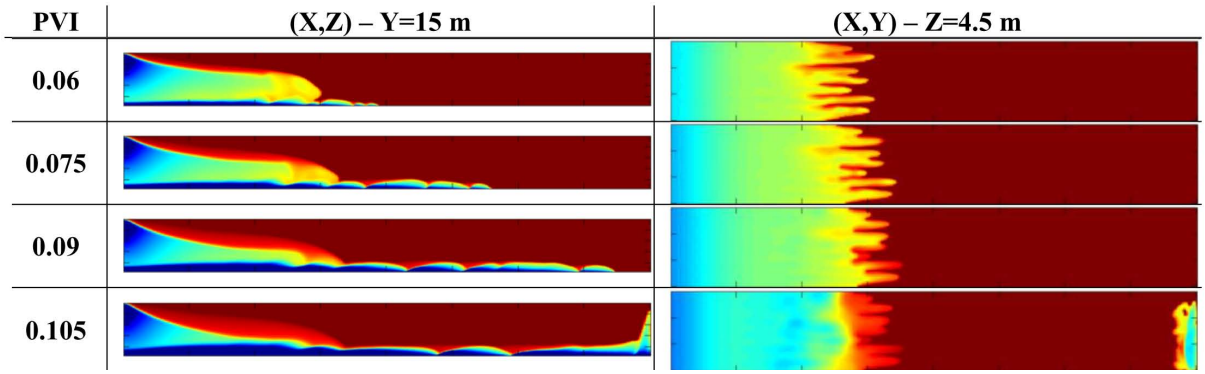

Figure 5—Water saturation in 2D vertical and horizontal cross-sections for a ‘gravity-dominant’ case, with ridge instabilities: Q=6 m³/day, Δρ=100 kg/m³, k_v/k_h=0.3

The selected 3D cases that illustrate the different flow patterns share the following common features: homogeneous permeability field, viscosity ratio (M=200), capillary pressure $p_{c,low}$, and reservoir sector of dimensions 200 m x 30 m x 6 m. We show the water saturation maps at 3 different PVI (Pore Volume Injected) before breakthrough and at another PVI just after breakthrough. A strong water coning effect at the producer is noticeable for all cases. Note that if the aspect ratio of 2D horizontal cross-sections is respected, this is not the case for 2D vertical cross-sections. All the water saturation maps displayed in this paper share the same color scale, provided at the bottom of *Figure 4*.

‘Gravity-dominant’ flow regime

When the gravity effects dominate – due to a large fluid density difference and / or a low injection flow rate and / or a high k_v/k_h ratio, the injected water rapidly migrates to the bottom of the reservoir and forms a gravity tongue that attenuates or even kills the potential viscous instabilities. The flow pattern is characterized by a fully-developed gravity tongue that propagates along the bottom of the reservoir, leaving a large part of the reservoir unswept, as shown in *Figure 4*.

With ridge instabilities. In a previous numerical study using a hybrid finite-difference/particle-tracking technique [10], it was observed in some cases that the gravity tongue displays a ‘ridge instability’ phenomenon, whereby *"the gravity layer breaks up into smaller sections with a ridge-like appearanc"e.* This may be attributed to an interaction between gravity tonguing and viscously unstable flow. Interestingly,

using high-order control-volume techniques, some of our simulated cases also exhibit such ridge instabilities, as shown in *Figure 5*. To our knowledge, however, this phenomenon has not been confirmed experimentally yet.

Transition flow regime

In the transition regime, the balance between viscous and buoyancy effects results in the phenomenon shown in *Figure 6* and described below:

- At early times (before PVI=0.1 for the selected case), viscous effects are preponderant and several viscous fingers are initiated laterally; meanwhile, in a vertical cross-section like that of *Figure 6* (left), we observe only one dominant viscous finger.
- At intermediate times (between PVI=0.1 and PVI=0.15), the buoyancy effects become noticeable: a thin gravity tongue starts to form and propagates rapidly, but the dominant viscous finger in the vertical cross-section of *Figure 6* (left) remains ahead of the gravity tongue.
- At later times, the effect of segregation is more pronounced and the gravity tongue propagates faster than the dominant viscous finger. Finally, just before breakthrough, the tip of the gravity tongue (red arrow 'GT') and the tip of the dominant viscous finger (green arrow 'VF') reach the producer almost simultaneously. It leads to an optimum in terms of breakthrough sweep efficiency, as the reservoir is not only swept in its bottom section by the gravity tongue but also in its middle section by the dominant viscous finger.

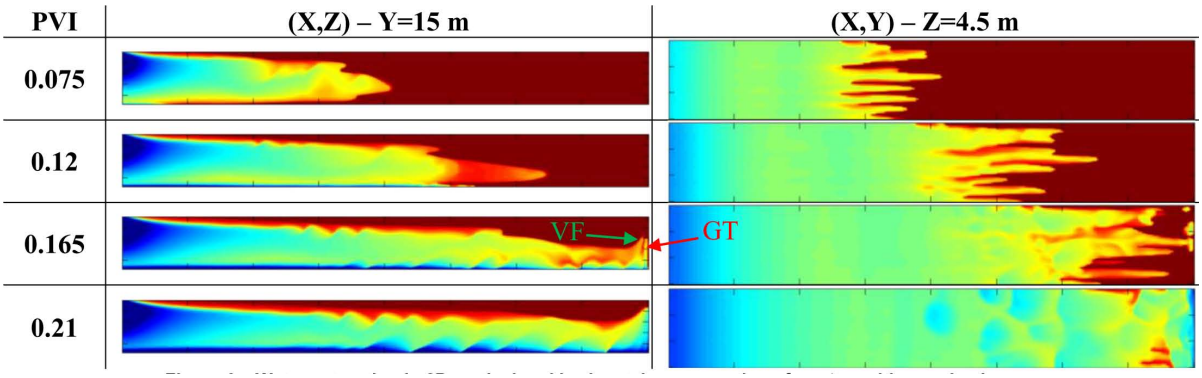

Figure 6—Water saturation in 2D vertical and horizontal cross-sections for a 'transition regime' case: Q=12 m³/day, Δρ=50 kg/m³, k_v/k_h=0.3

'Viscous-dominant' flow regime

When the viscous forces are preponderant (e.g. due to small Δρ and / or high Q and / or low k_v/k_h), the gravity tongue is very weak or non-existent, and the flow pattern in a vertical cross-section is often characterized by one dominant viscous finger, as shown in *Figure 7*. However, after a certain time – possibly after water breakthrough, a very thin yet noticeable gravity tongue starts to form (cf. saturation map at PVI=0.165).

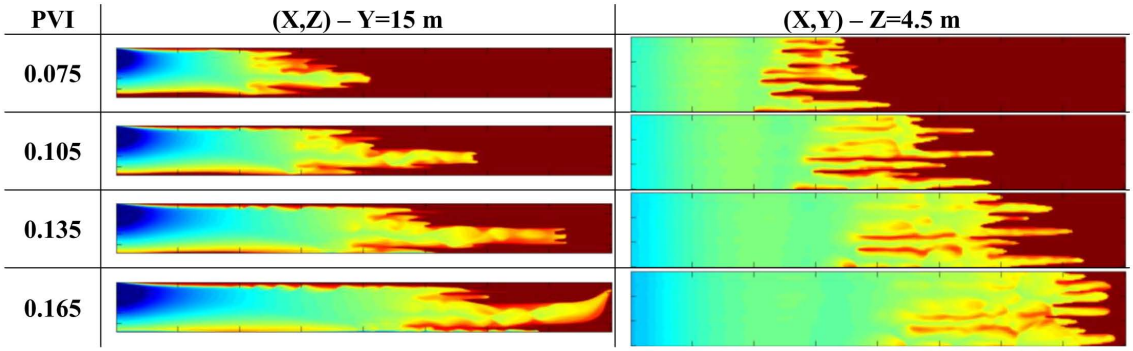

Figure 7—Water saturation in 2D vertical and horizontal cross-sections for a 'viscous-dominant' case: Q=18 m³/day, Δρ=100 kg/m³, k_v/k_h=0.1

Estimation of water breakthrough time

In this section, we focus on the water breakthrough time expressed in PVI, denoted by WBT. Since the two fluids are nearly incompressible, the WBT is almost proportional to the oil recovery factor at breakthrough.

First of all, we check if we can use 2D vertical simulations to compute the WBT accurately. Next, we determine if the viscous-to-gravity ratio and the viscosity ratio are relevant enough to estimate the WBT. The results being negative, we then analyze specifically how the WBT is impacted by the main physical and geological parameters.

The default values used in the simulations are the following: viscosity ratio of 200, fluid density difference of 100 kg/m³, capillary pressure given by $p_{c,low}$, homogeneous permeability field with vertical-to-horizontal permeability ratio of 0.3, and reservoir sector dimensions of 200 m x 30 m x 6 m. The $R_{v/g}$ calculation is based on an average Darcy velocity U, defined by the injection flow rate over the area of the transverse cross-section (total reservoir thickness by domain width).

Comparison between 2D & 3D estimations of the WBT

We first compare 2D and 3D estimations of the WBT on 27 simulation cases: 9 injection flow rates (from 2 to 18 m³/day) for three viscosity ratios (100, 200 and 400). The results are plotted in *Figure 8 (a)*, where each color corresponds to a specific viscosity ratio and each symbol to 2D ('+') or 3D ('*') results:

- Large discrepancies occur between 2D and 3D results: the average relative error in WBT using a 2D geometry is more than 9.5 %, with a maximum reaching 17.3%.
- The water breakthrough always occurs earlier in 3D, resulting in a lower oil recovery factor at breakthrough. Two main causes were identified:
  - Transverse viscous fingering may occur in 3D, as shown in *Figure 8 (b)*, but such effect cannot be captured in 2D.
  - The spreading of the gravity tongue is sometimes more pronounced in 3D than in 2D, as illustrated in *Figure 8 (c)*. In this case, the development of ridge instabilities in the gravity tongue is clearly impacted by 3D effects, as exhibited in *Figure 8 (d)*. It is worth noting that the simulations of ridge instabilities in were performed in 2D; to our knowledge, we here present the first 3D simulations of this phenomenon, suggesting the importance of 3D effects on the flow characteristics.

Consequently, three-dimensional simulations are required to reproduce accurately the water breakthrough time: subsequent simulations will thus be performed in 3D.

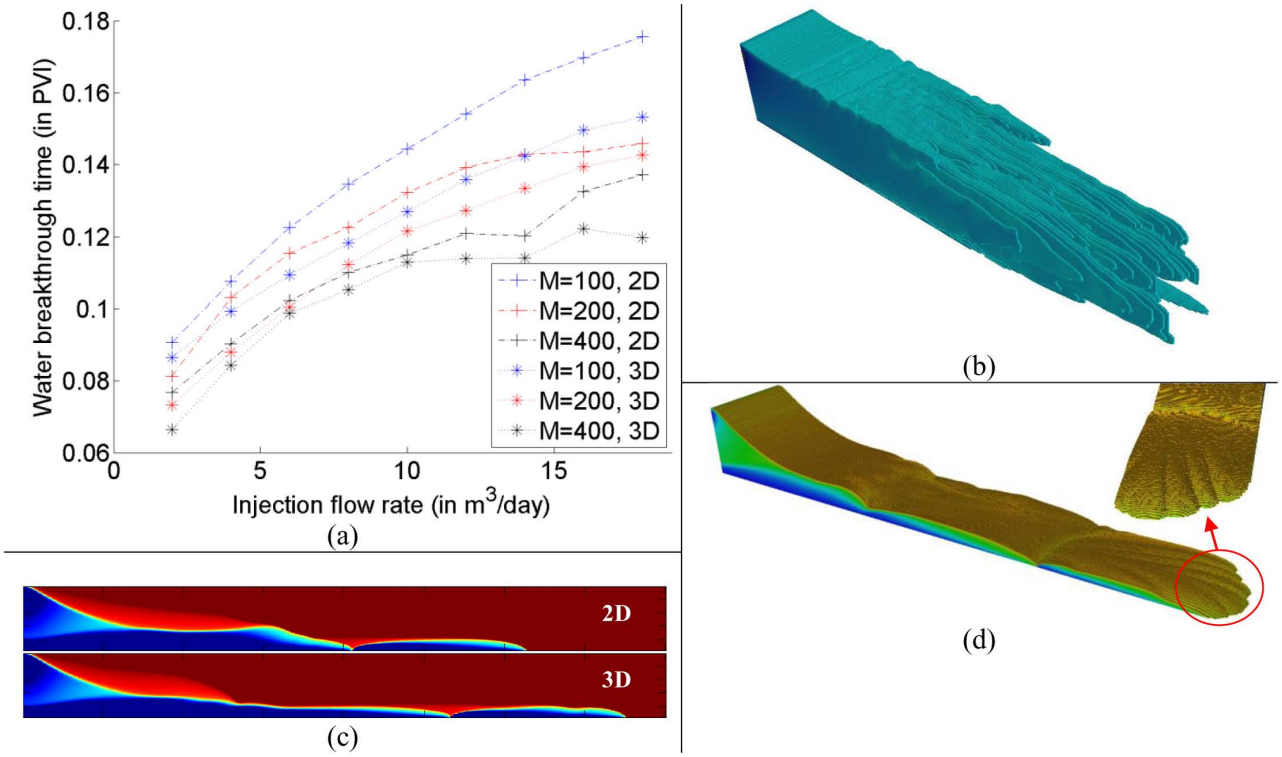

Figure 8—(a) WBT vs. injection flow rate for different viscosity ratios, using 2D and 3D simulations. (b) 3D view of viscous fingers at PVI=0.105 for M=400 & Q=18 m³/day. (c) Water saturation at PVI=0.105 in a 2D vertical cross-section (Y=15 m) for M=100 & Q=8 m³/day, using 2D (top) and 3D (bottom) simulations. (d) 3D views of the gravity tongue for the case considered in (c)

Dependence of the WBT on $R_{v/g}$

We now evaluate in 3D how the WBT depends on the viscous-to-gravity ratio $R_{v/g}$, for a constant viscosity ratio of 200:

- First, we perform eight simulations with the same $R_{v/g}$ (equal to $4.53.10^{-4}$), by varying only the fluid density difference (from 25 to 200 kg/m³) and the injection flow rate (from 2 to 16 m³/day). The calculated values of WBT are reported in *Figure 9 (a)* and the saturation maps for the two extreme cases are shown in *Figure 10*: the WBT varies from 0.108 PVI (high Q, high Δρ) to 0.126 PVI (low Q, low Δρ), which represents a difference of 17 % for the same set of parameters ($R_{v/g}$, M).
- Secondly, we plot in *Figure 9 (b)* the WBT when varying the fluid density difference (from 25 to 200 kg/m³), the injection flow rate (from 2 to 18 m³/day), the anisotropy ratio k_v/k_h (0.1, 0.3 & 0.9) and the reservoir sector dimensions (200 m x 30 m x 6 m, 100 m x 30 m x 6 m and 200 m x 30 m x 3 m). For these 71 simulations, the capillary pressure curve was set to $p_{c,low}$ and the permeability field was homogeneous.
    - Qualitatively, the higher the $R_{v/g}$, the higher the WBT in PVI. Indeed, when starting from a gravity-dominant case, increasing the viscous effects improves the sweep efficiency and so delays the WBT. However, at high enough $R_{v/g}$ this trend disappears and the WBT even slightly diminishes. This behavior will be explained further below, e.g. when analyzing the influence of injection flow rate and fluid density difference on the WBT.

- At a fixed value of $R_{v/g}$, the maximum absolute difference in WBT is always close to 0.018 PVI. Thus, the maximum relative difference increases as $R_{v/g}$ diminishes, from 9.9% at $R_{v/g}=1.36.10^{-3}$ to 25.5% at $R_{v/g}=1.13.10^{-4}$.
- For the same $R_{v/g}$, the highest value of WBT always corresponds to the lowest fluid density difference, as observed in *Figure 10*. Such behavior cannot be explained easily, but it is probably due to the complex interaction between viscous effects and gravity tonguing, resulting in some nonlinear effects (w.r.t. Q, Δρ,…) on the gravity tongue propagation.

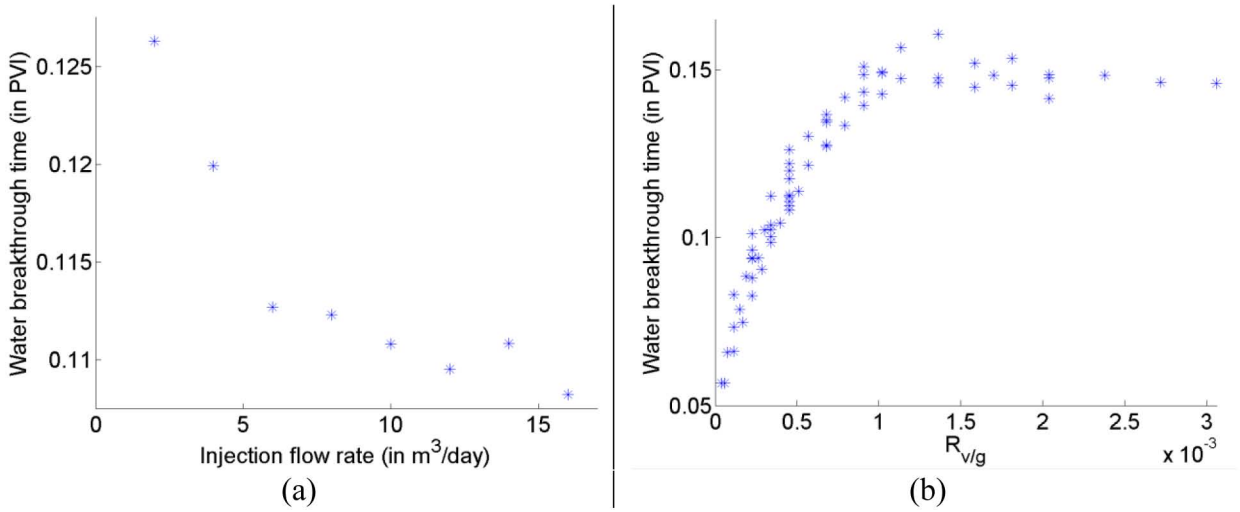

Figure 9—(a) WBT vs. injection flow rate for a fixed set of parameters ($R_{v/g}$, M). (b) WBT vs. $R_{v/g}$ for M=200

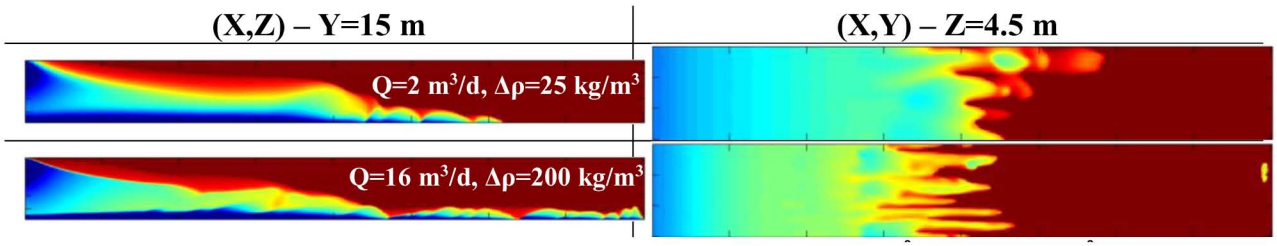

Figure 10—Water saturation at PVI=0.105 in 2D vertical and horizontal cross-sections for Q=2 m³/day, Δρ=25 kg/m³ (top) and Q=16 m³/day, Δρ=200 kg/m³ (bottom)

Although the WBT globally increases with $R_{v/g}$, significant discrepancies are observed for the same set of parameters ($R_{v/g}$, M): the WBT cannot be considered a function of these two dimensionless parameters only.

Consequently, we decided to analyze in more details how the WBT is impacted by the different physical and geological parameters: injection flow rate, domain aspect ratio, viscosity ratio, fluid density difference, capillary pressure curve, vertical-to-horizontal permeability ratio and horizontal permeability correlation length.

Influence of the injection flow rate and the viscosity ratio on the WBT

The WBT for different injection flow rates (from 2 to 18 m³/day) and viscosity ratios (100, 200 and 400) are given in *Figure 11*:

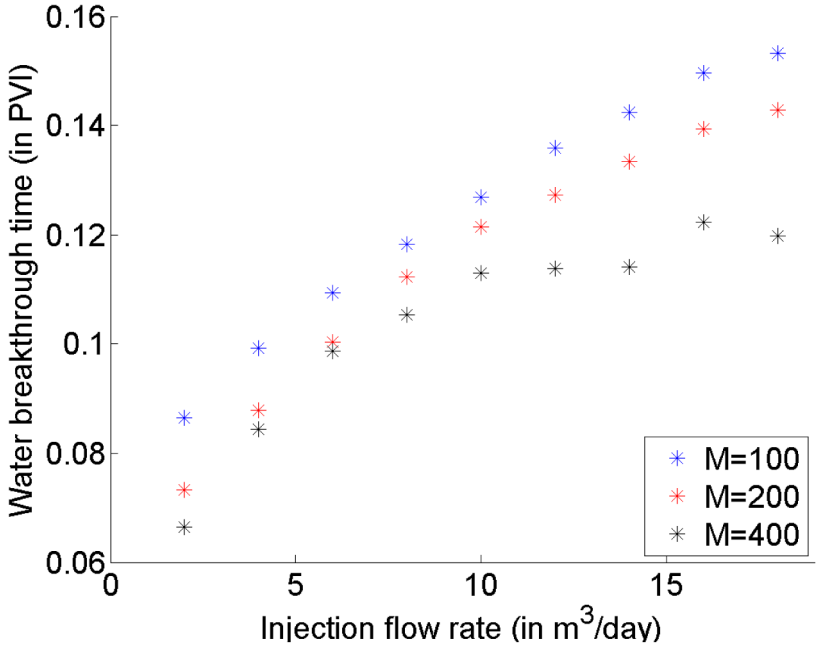

Figure 11—WBT vs. injection flow rate for three viscosity ratios

- We first focus on the influence of the injection flow rate using default values for all parameters (red points, with M=200): the higher the injection flow rate, the higher the WBT expressed in PVI. The water saturation maps in a 2D vertical cross-section shown in *Figure 12* at the same PVI for Q=2 & 18 m³/day explain it clearly: a low injection velocity leads to the development of a thin gravity tongue reaching the producer rapidly, whereas a higher injection flow rate increases the viscous effects and improves the sweep efficiency, thus delaying the breakthrough.
- The previous observation on the impact of injection flow rate is also valid for lower M; for higher M, the trend is not so clear when reaching high injection flow rate, due to viscous instabilities occurring near the producer just before breakthrough, as shown in *Figure 13*: for Q=16 m³/day, three fingers reach the producer at breakthrough, when there are only two for Q=14 & 18 m³/day. This phenomenon is case-dependent, and is probably provoked by very small perturbations, possibly due to inherent numerical errors.
- For a fixed injection flow rate, the higher the viscosity ratio, the lower the WBT. Indeed a higher M leads to a lower front saturation and a higher front velocity, while favoring the development of transverse viscous fingers. This leads to a lower sweep efficiency and a lower WBT, as illustrated in *Figure 14* providing a comparison of saturation maps for different M (100 & 400) but constant Q=18 m³/day.

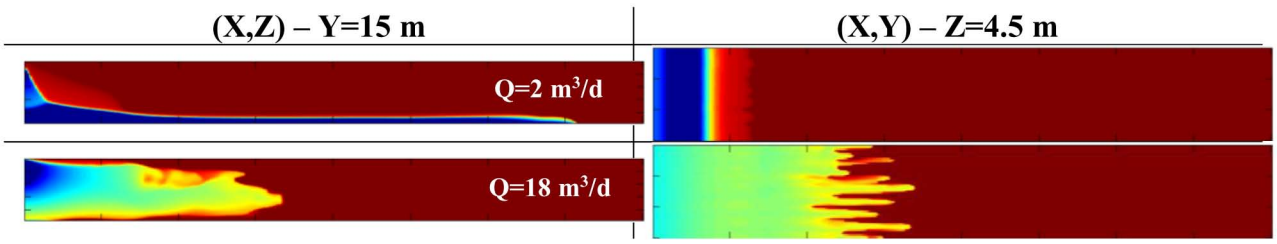

Figure 12—Water saturation at PVI=0.06 in 2D vertical and horizontal cross-sections for Q=2 (top) or 18 m³/day (bottom) and M=200

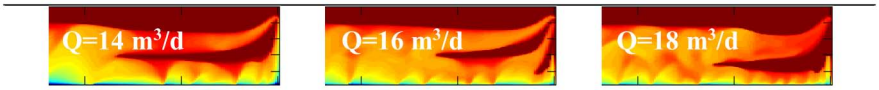

Figure 13—Water saturation at PVI=0.135 in a 2D vertical cross-section (restricted view near the producer, with the same axis scale as in *Figure 12*) for Q=14, 16 & 18 m³/day (left to right) and M=400

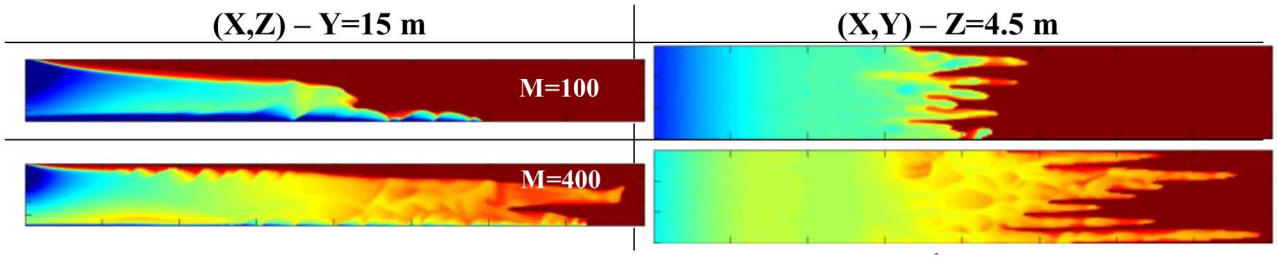

Figure 14—Water saturation at PVI=0.12 in 2D vertical and horizontal cross-sections for Q=18 m³/day and M=100 (top) or 400 (bottom)

Influence of the injection flow rate and the fluid density difference on the WBT

The WBT for different injection flow rates and density differences between oil and water (50, 100 and 200 kg/m³) are given in *Figure 15*:

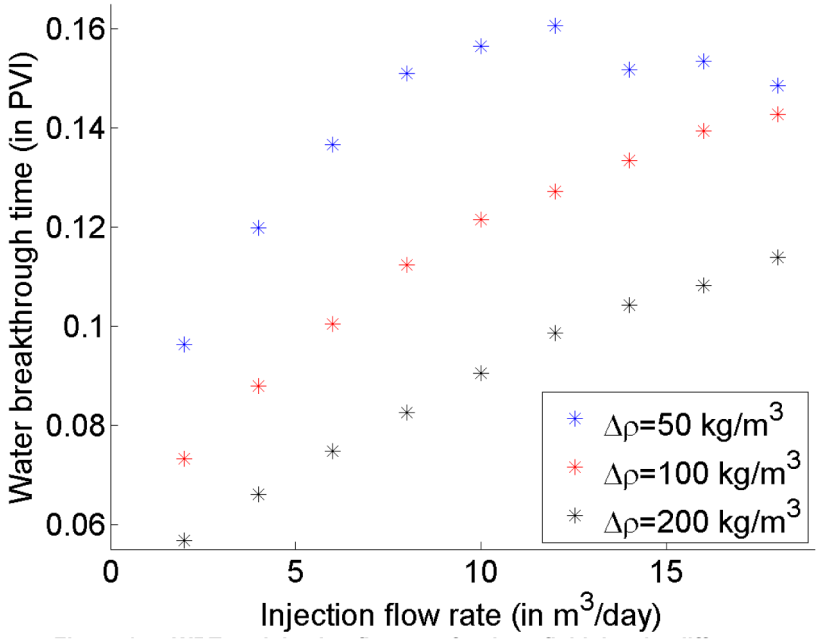

Figure 15—WBT vs. injection flow rate for three fluid density differences

- The simulation results in red (using default parameters) correspond to those already presented in red in *Figure 11* and interpreted previously – they will also be recalled in the following plots of WBT vs. injection flow rate for all the other sensitivity studies.
- For a fixed injection flow rate, the higher the fluid density difference, the lower the water breakthrough time. Indeed, a higher Δρ leads to a stronger gravity tongue, resulting in a lower WBT. This is clearly illustrated in *Figure 16*, with the saturation maps for different Δρ (50 & 200 kg/m³) but constant Q=12 m³/day.
- The positive impact of the injection flow rate on the WBT when using default parameters (red points in *Figure 15*, with Δρ=100 kg/m³) is also seen for higher Δρ. However, for lower Δρ=50 kg/

m^3, we observe an optimum injection flow rate at Q_{opt}=12 m^3/day. This optimum can be interpreted by comparing the flow patterns around Q_{opt} in *Figure 17*:

- The optimum injection flow rate corresponds to a transition flow regime, where the gravity tongue and the main viscous finger reach the producer quasi-simultaneously, as shown in *Figure 17* (middle).
- For a flow rate value lower than Q_{opt} (cf. top of *Figure 17* for Q=10 m^3/day), the flow regime is more 'gravity-dominant', with a slightly stronger gravity tongue.
- For a flow rate value higher than Q_{opt} (cf. bottom of *Figure 17* for Q=14 m^3/day), the flow regime becomes more 'viscous-dominant'.

We do not observe any optimum injection flow rate for the two higher density differences simply because the gravity effects remain preponderant up to the maximum tested flow rate. By increasing the injection velocity further, the flow regime would progressively shift from 'gravity-dominant' to 'viscous-dominant', going through a transition regime with an optimum in WBT. This general remark also applies to the other sensitivity studies performed thereafter.

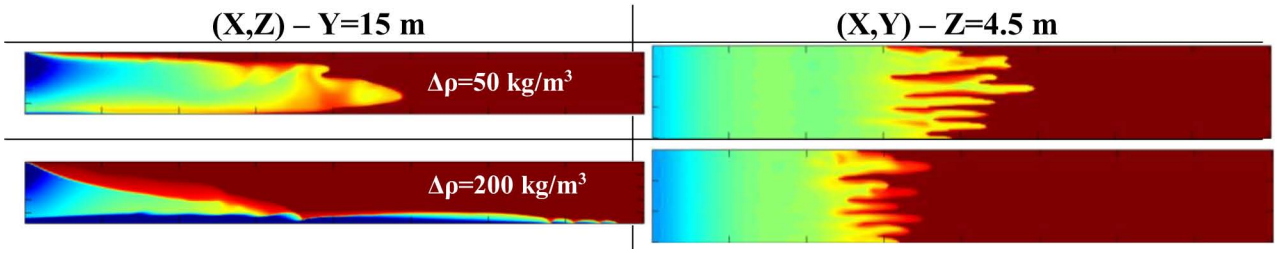

Figure 16—Water saturation at PVI=0.09 in 2D vertical and horizontal cross-sections for Q=12 m^3/day and Δρ=50 (top) or 200 kg/m^3 (bottom)

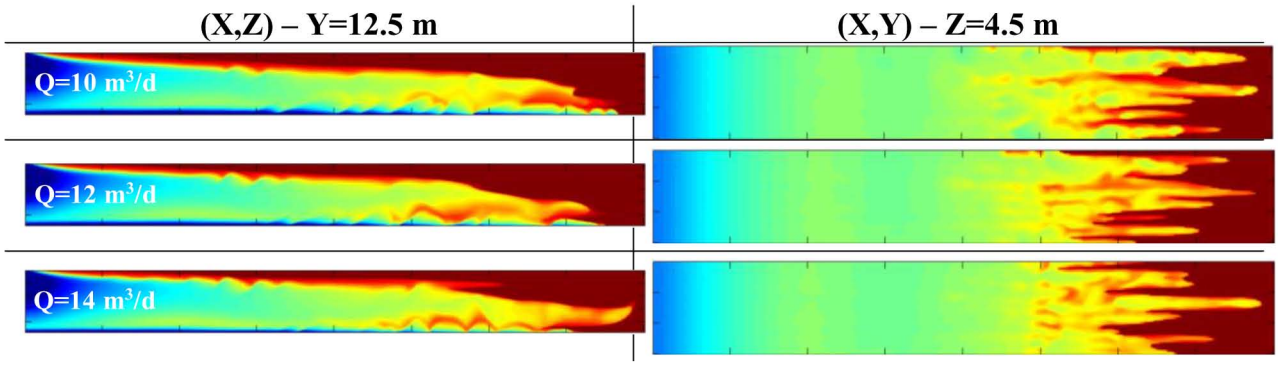

Figure 17—Water saturation at PVI=0.15 in 2D vertical and horizontal cross-sections for Q=10, 12 & 14 m^3/day (top to bottom) and Δρ=50 kg/m^3

Influence of the injection flow rate and the permeability anisotropy on the WBT

The WBT for different injection flow rates and vertical-to-horizontal permeability ratios (0.1, 0.3 and 0.9) are given in *Figure 18*:

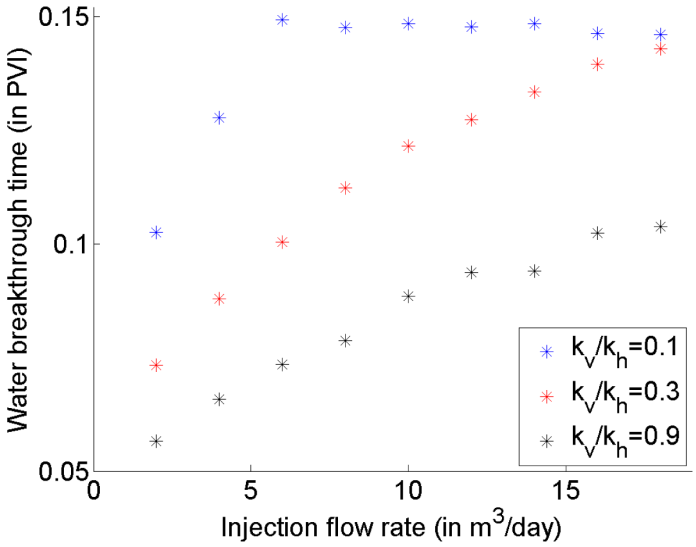

Figure 18—WBT vs. injection flow rate for three permeability anisotropy ratios

- For a fixed injection flow rate, the higher the vertical-to-horizontal permeability ratio, the lower the water breakthrough time. Indeed, like in the previous sensitivity study on the fluid density difference, a higher k_v/k_h leads to a stronger gravity tongue and a lower WBT. This is illustrated by the saturation maps in *Figure 19*, for different k_v/k_h (0.1 & 0.9) but constant Q=6 m^3/day.
- The positive impact of the injection flow rate on the WBT when using default parameters (red points in *Figure 18*, with k_v/k_h=0.3) is also confirmed for higher k_v/k_h. However, for lower k_v/k_h=0.1, we observe an optimum injection flow rate at Q_{opt}=6 m^3/day corresponding to the transition flow regime, as illustrated in *Figure 20*. The comments made for *Figure 17* also apply here.

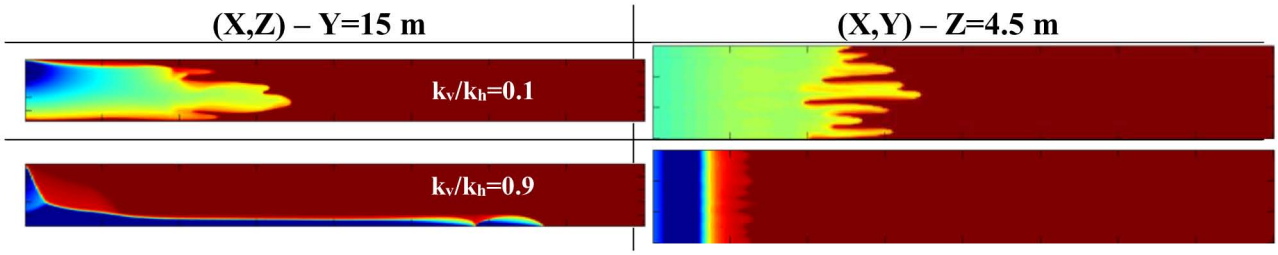

Figure 19—Water saturation at PVI=0.06 in 2D vertical and horizontal cross-sections for Q=6 m^3/day and k_v/k_h=0.1 (top) or 0.9 (bottom)

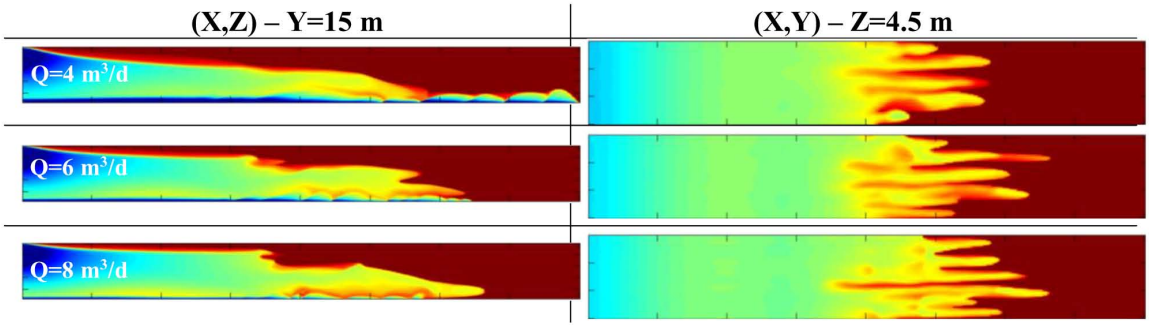

Figure 20—Water saturation at PVI=0.12 in 2D vertical and horizontal cross-sections for Q=4, 6 & 8 m^3/day (top to bottom) and k_v/k_h=0.1

Influence of the injection flow rate and the domain aspect ratio on the WBT

The WBT for different injection flow rates and domain dimensions – base case (200 m x 30 m x 6 m), reservoir height H divided by 2 (200 m x 30 m x 3 m) and inter-well distance L divided by 2 (100 m x 30 m x 6 m) – are given in *Figure 21*:

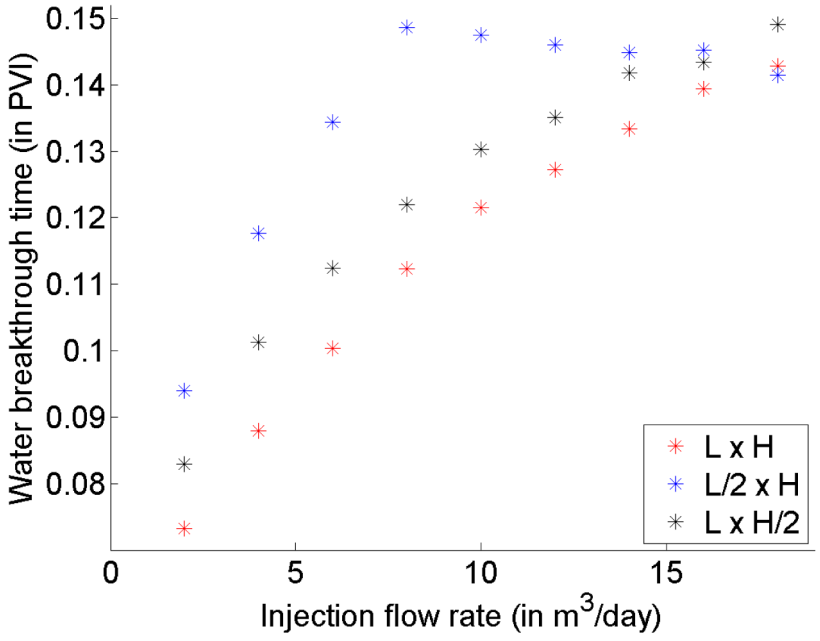

Figure 21—WBT vs. injection flow rate for three reservoir dimensions

- For a given injection flow rate, we observe a higher WBT when the reservoir height decreases while the inter-well distance remains the same. Indeed, over the range of tested flow rates, the flow regime is gravity-dominant: when the reservoir height goes from 6 to 3 m, the thickness of the gravity tongue does not diminish in the same proportion (we note that the Darcy velocity in the second case is higher, which increases the viscous effects). Therefore, the unswept part of the reservoir decreases, as illustrated in *Figure 22* with the saturation maps for Q=8 m^3/day and H=6 m (top) or H=3 m (middle).
- For all injection flow rates except the highest one, we observe a higher WBT when the inter-well distance decreases while the reservoir height remains the same. Indeed, for the same PVI, the gravity effects have 'less time' to counterbalance the viscous forces, the reservoir domain is thus better swept, which increases the WBT, as shown in *Figure 22* (top vs. bottom). Note that here the same injection flow rate results in the same Darcy velocity.
- We observe an optimum injection flow rate in terms of WBT at Q_{opt}=8 m^3/day when the inter-well distance is set to 100 m. As already explained, this is due to the transition of flow regimes occurring around Q_{opt}.

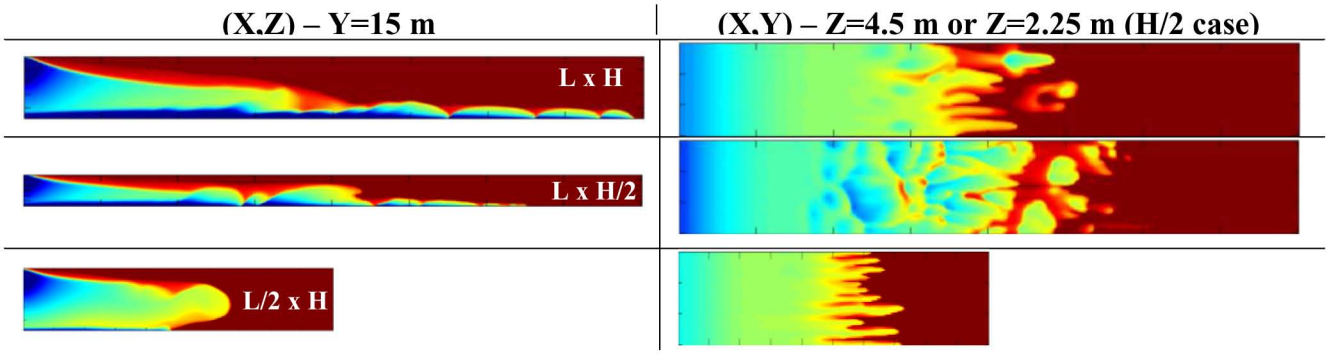

Figure 22—Water saturation at PVI=0.105 in 2D vertical and horizontal cross-sections for Q=8 m³/day and different domain aspect ratios

Influence of the injection flow rate and the capillary pressure on the WBT

The WBT for different injection flow rates and capillary pressure curves ($p_{c,low}$, $p_{c,medium}$ & $p_{c,high}$) are given in *Figure 23*:

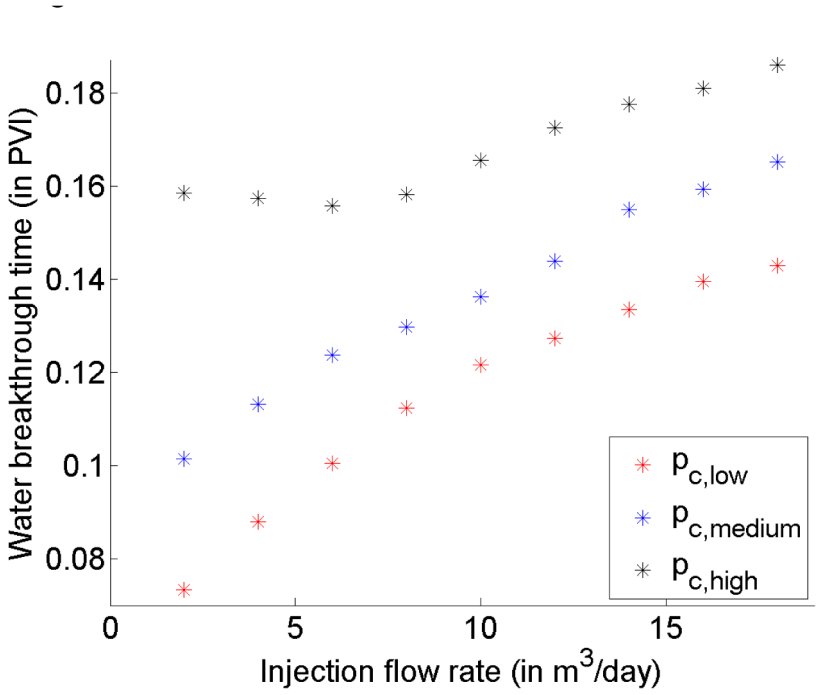

Figure 23—WBT vs. injection flow rate for three capillary pressure curves

- For a fixed injection flow rate, the higher the capillary pressure, the higher the WBT. Indeed, a higher capillary pressure leads to a stronger 'diffusion effect' due to spontaneous imbibition, as observed in *Figure 24*, resulting in a better sweep efficiency and a higher WBT.
- The positive impact of the injection flow rate on the WBT when using default parameters (red points in *Figure 23*, with $p_{c,low}$) is also observed for $p_{c,medium}$. However for $p_{c,high}$, we observe an optimum injection flow rate Q_{opt}=6 m³/day that minimizes the WBT. To explain this, we note that for all the cases, while the gravity effects are dominant, there is also a competition between viscous and capillary effects. The saturation maps in *Figure 25* show that for the same PVI:
  - by reducing the injection flow rate, spontaneous imbibition occurs over a longer time period, which tends to improve the sweep efficiency and thus increases the WBT

- by increasing the injection flow rate, thus the viscous effects, the zone near the injector tends to be better swept while the gravity tongue is locally more disturbed and slightly thicker, which leads to a higher WBT as well.

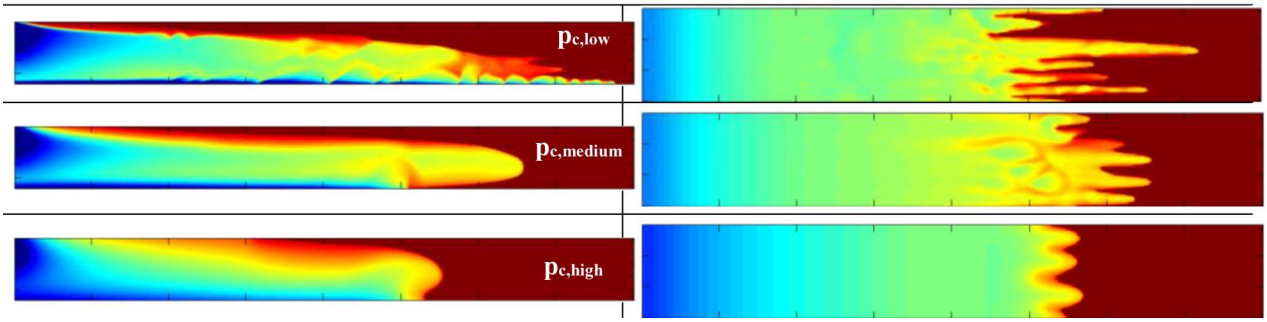

Figure 24—Water saturation at PVI=0.135 in 2D vertical and horizontal cross-sections for Q=18 m^3/day and $p_{c,low}$, $p_{c,medium}$ or $p_{c,high}$ (top to bottom)

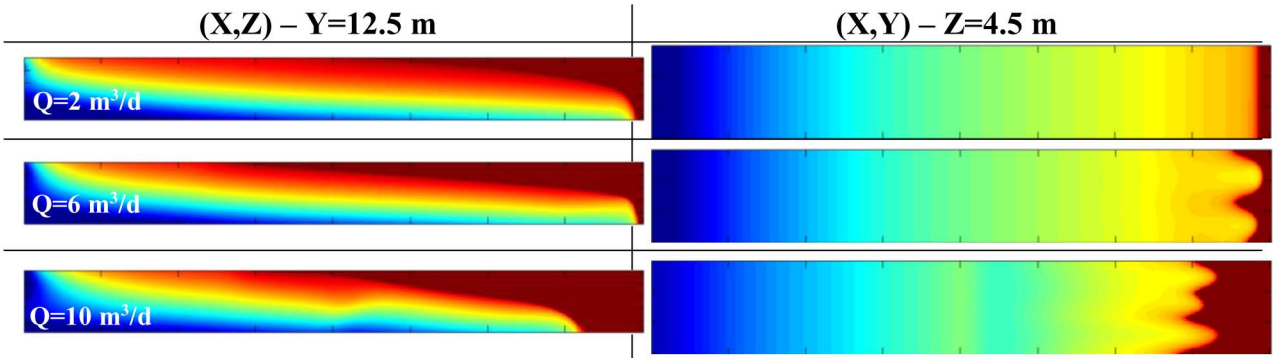

Figure 25—Water saturation at PVI=0.15 in 2D vertical and horizontal cross-sections for Q=2, 6 & 10 m^3/day (top to bottom) and $p_{c,high}$

Influence of the injection flow rate and the horizontal permeability correlation length on the WBT

The WBT for different injection flow rates when using a homogeneous permeability field or heterogeneous fields with different horizontal correlation lengths (2, 5 & 10 m, as illustrated in *Figure 2*), are given in *Figure 26*:

- For all the permeability fields, the higher the injection flow rate, the higher the WBT, as observed in *Figure 11* and already explained.
- For a fixed injection flow rate, the maximum WBT is always obtained with the homogeneous permeability field: this is due to the formation of preferential paths in the heterogeneous fields, as shown in *Figure 27*. There is however no direct link between the WBT and the horizontal correlation length: indeed, the field with l_{corr}=5 m always yields a lower WBT than the field with l_{corr}=2 m, but the field with l_{corr}=10 m leads to a higher WBT than the field with l_{corr}=5 m, or even l_{corr}=2 m when $Q \leq 6$ m^3/day. Therefore, the impact of the permeability correlation length appears to be case-dependent, which is attributed to complex interactions between heterogeneity, buoyancy and viscous effects. Nevertheless, further analysis based on multiple realizations of each permeability distribution and variogram may help identify some stochastic trends. This is left for future work.

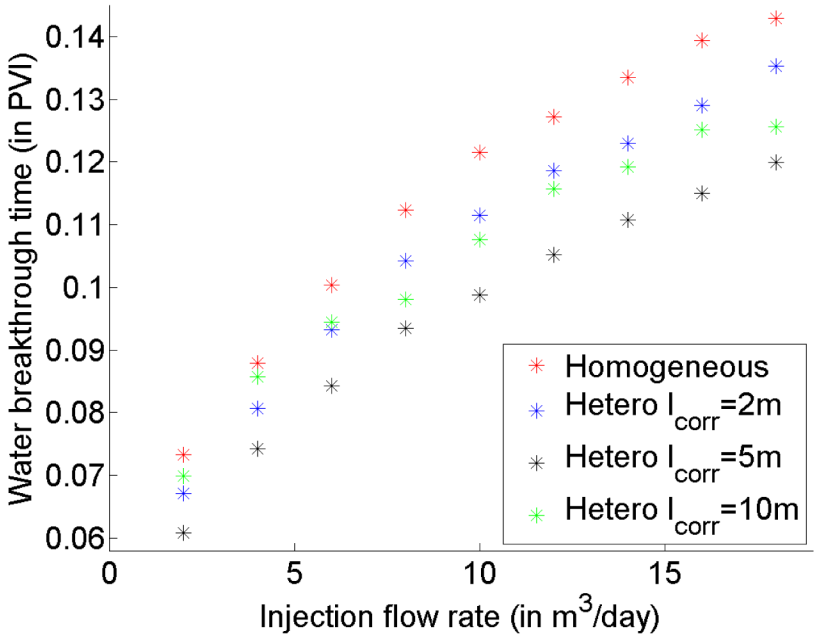

Figure 26—WBT vs. injection flow rate for different horizontal permeability correlation lengths

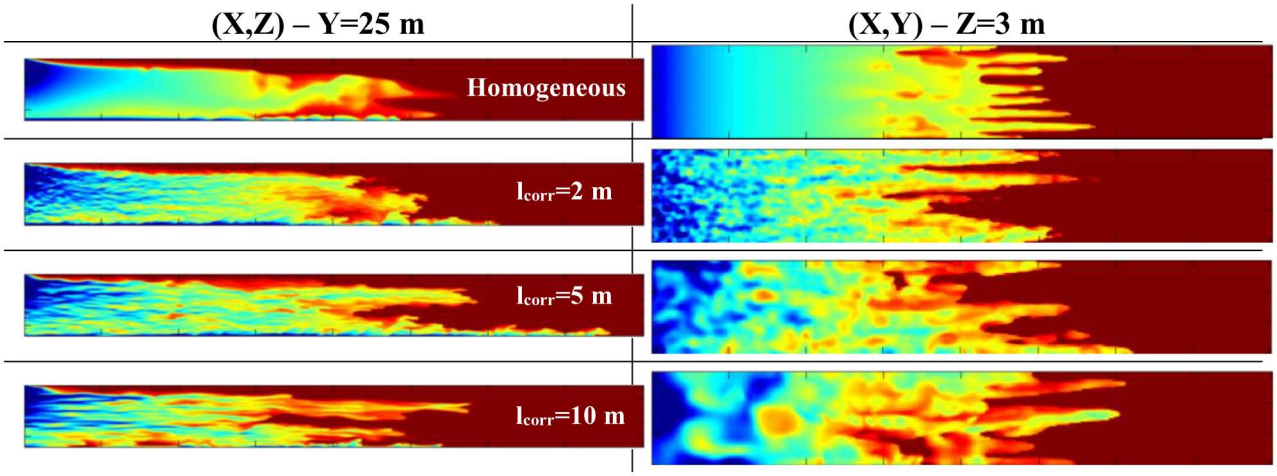

Figure 27—Water saturation at PVI=0.105 in 2D vertical and horizontal cross-sections for different horizontal permeability correlation lengths and Q=18 m³/day

Estimation of oil recovery during the fully-developed regime

In this section, we focus on the oil recovery during the fully-developed regime, meaning after water breakthrough. We first check if we can use 2D vertical simulations to compute accurately the oil recovery factor, denoted by RF, at different PVI after breakthrough. Next, we determine to what extent the viscous-to-gravity ratio $R_{v/g}$ and the viscosity ratio M are relevant to estimate the RF during the fully-developed regime. This analysis will be performed for different levels of capillary pressure and considering both homogeneous and heterogeneous permeability fields.

Comparison between 2D & 3D estimations of oil recovery after breakthrough

We compare in *Figure 28* the RF estimations in 2D and 3D at PVI=0.4 *(a)*, PVI=0.7 *(b)* and PVI=1 *(c)*, based on 27 simulation cases: three injection flow rates (4.5, 9 and 18 m³/day), three fluid density differences (50, 100 and 200 kg/m³) and three viscosity ratios (100, 200 and 400). The 27 cases share the following features: homogeneous permeability field with vertical-to-horizontal permeability ratio of 0.3, capillary

pressure curve $p_{c,low}$ and reservoir dimensions of 200 m x 30 m x 6 m. Each color corresponds to a specific viscosity ratio, and different symbols are used for 2D ('+') or 3D ('*') results.

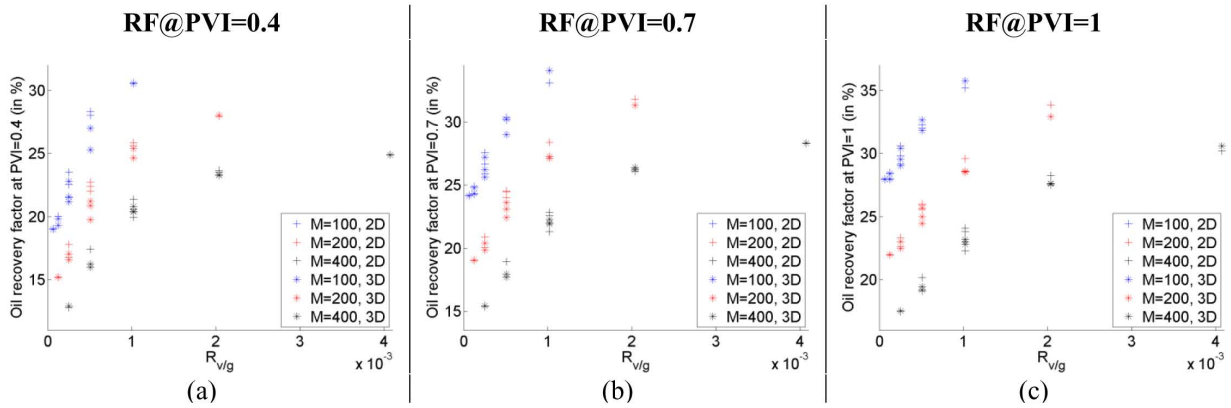

Figure 28—Oil recovery factor vs. viscous-to-gravity ratio for different viscosity ratios, using 2D and 3D simulations, at PVI=0.4 (a), PVI=0.7 (b) and PVI=1 (c)

Minor differences occur between 2D and 3D results: in average, the estimation of oil recovery factors in 2D only differs from 3D by 3.1 % at PVI=0.4 and by 1.5% at PVI=1. Meanwhile, the maximum error decreases from 11.6% to 4.5% (cf. *Table 1*).

Table 1—Average and maximum errors of RF estimation in 2D vs. 3D, at different PVI

	Average error	Maximum error
PVI=0.4	3.1 %	11.6%
PVI=0.7	2.0 %	7.1%
PVI=1.0	1.5 %	4.5 %

As seen previously, some of the complex flow behaviors occurring before breakthrough may not be correctly represented by 2D simulations. But shortly after breakthrough, the flow pattern is generally dominated by a fully-developed gravity tongue and the importance of 3D effects diminishes, thus 2D simulations become more and more accurate. Even for the most unstable case – with the highest $R_{v/g}$ and M, the 2D simulation is able to reproduce rather accurately the 3D late-time results, as shown by the comparison of 2D and 3D saturation maps in *Figure 29*.

Consequently, we decided to estimate the oil recovery factors in the fully-developed regime by running only 2D simulations, which allows a significant gain in computational time.

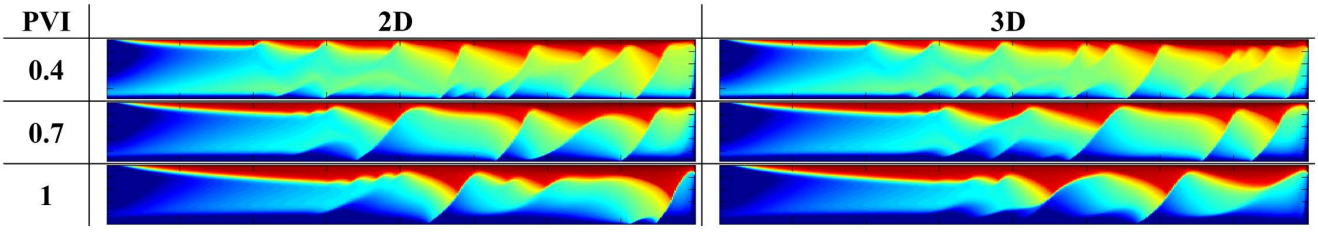

Figure 29—Water saturation at different PVI in a 2D vertical cross-section for Q=18 m³/day, M=400 & Δρ=50 kg/m³, using 2D and 3D simulations

Dependence of the oil recovery after breakthrough on $R_{v/g}$ and M for low capillary effects

We here study how the oil recovery after breakthrough depends on the viscous-to-gravity ratio and the viscosity ratio, when using the capillary pressure curve $p_{c,low}$.

Variation of all the parameters – homogeneous case. A total of 1350 two-dimensional simulations were run to estimate the RF at different PVI, by varying all the following parameters:

- the injection flow rate Q: 10 values were tested, from 2 to 18 m^3/day
- the fluid density difference Δρ: 5 values were tested, namely 50, 75, 100, 150 and 200 kg/m^3
- the viscosity ratio M: 3 values were tested, namely 100, 200 and 400
- the vertical-to-horizontal permeability ratio k_v/k_h: 3 values were tested, namely 0.1, 0.3 and 0.9
- the domain aspect ratio: base case (200 m x 30 m x 6 m), reservoir height divided by 2 (200 m x 30 m x 3 m) and inter-well distance divided by 2 (100 m x 30 m x6 m)

For this sensitivity study, the homogeneous permeability field was used.
The oil recovery factors at three PVI (0.4, 0.7 & 1) are shown in *Figure 30*:

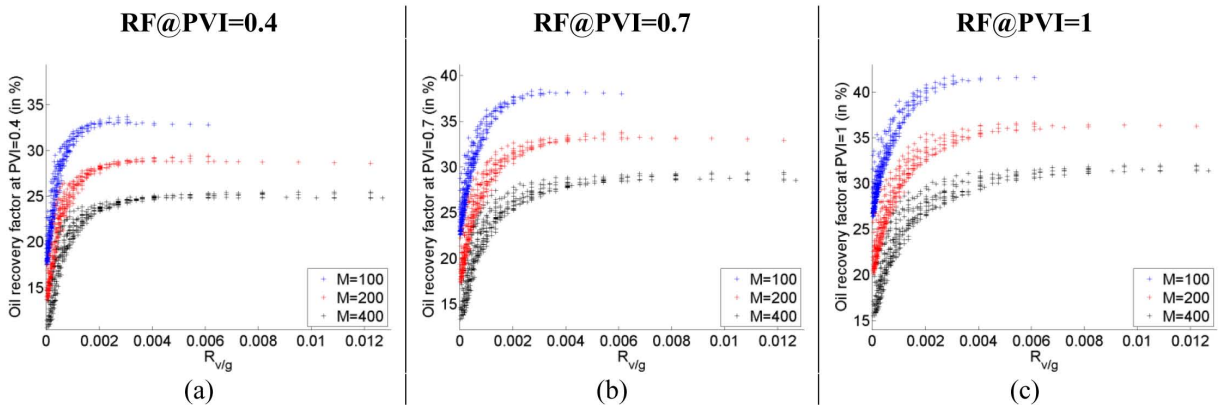

Figure 30—Oil recovery factor vs. viscous-to-gravity ratio for different viscosity ratios, when using $p_{c,low}$, for PVI=0.4 (a), PVI=0.7 (b) and PVI=1 (c)

- The dependence of the RF@PVI=0.4 upon $R_{v/g}$ and M only is quite well satisfied, although some dispersion is noticeable, especially at low $R_{v/g}$ (cf. *Figure 30* (a)).
- When the PVI increases, the dispersion associated with the RF dependence upon $R_{v/g}$ and M slowly increases, as suggested by *Figure 30 (b)* and *(c)*:
  - For the same set of ($R_{v/g}$, M), the mean dispersion of the RF, estimated in percentage point (pp), goes from 2 pp only at PVI=0.4, then 3 pp at PVI=0.7 and nearly 4 pp at PVI=1.
  - In *Figure 31*, we visualize the origin of this dispersion by plotting the evolution of the water saturation maps for two extreme cases that share the same $R_{v/g}$=0.001359 and M=400: the two cases only differ by their aspect ratio and their fluid density difference. The late-time flow patterns are very different: although one case is characterized by a strong gravity tongue that stabilizes progressively, the other case exhibits a gravity tongue with severe ridge instabilities, even at PVI=1.
  - We conclude that from a theoretical point of view $R_{v/g}$ and M are not sufficient to accurately predict the flow pattern after breakthrough. Nevertheless, in practice, the average level of dispersion is deemed acceptable for a first-order estimation of oil recovery.

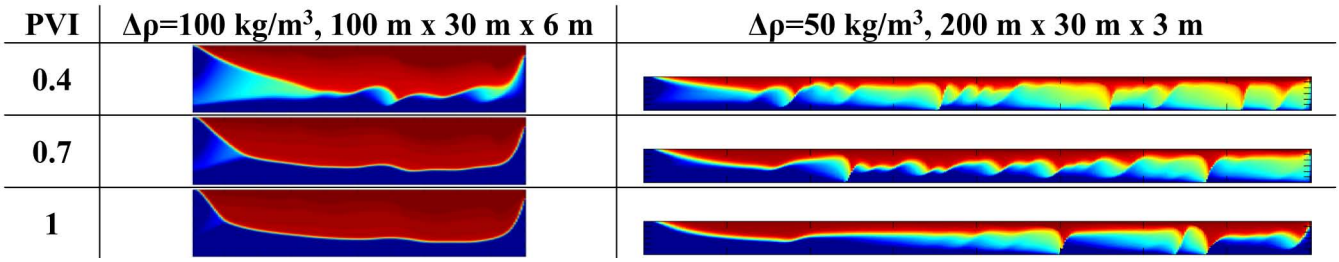

Figure 31—Water saturation maps at different PVI for two cases sharing the same set of parameters ($R_{v/g}$,M), Q=18 m³/day, M=400, k_v/k_h=0.9 but with Δρ=100 kg/m³ & 100 m x 30 m x 6 m (left) and Δρ=50 kg/m³ & 200 m x 30 m x 3 m (right)

Variation of all the parameters, except the aspect ratio – homogeneous case. Sometimes in the literature (e.g. [2] or [10]), the aspect ratio is considered as a separate dimensionless number: we thus plot in *Figure 32* the RF@PVI=1 when setting the reservoir domain dimensions to 200 m x 30 m x 6 m (a), 200 m x 30 m x 3 m (b) and 100 m x 30 m x 6 m (c). Except for case (a), the RF dispersion remains noticeable, therefore we do not observe any clear improvement by considering the domain aspect ratio as a separate parameter.

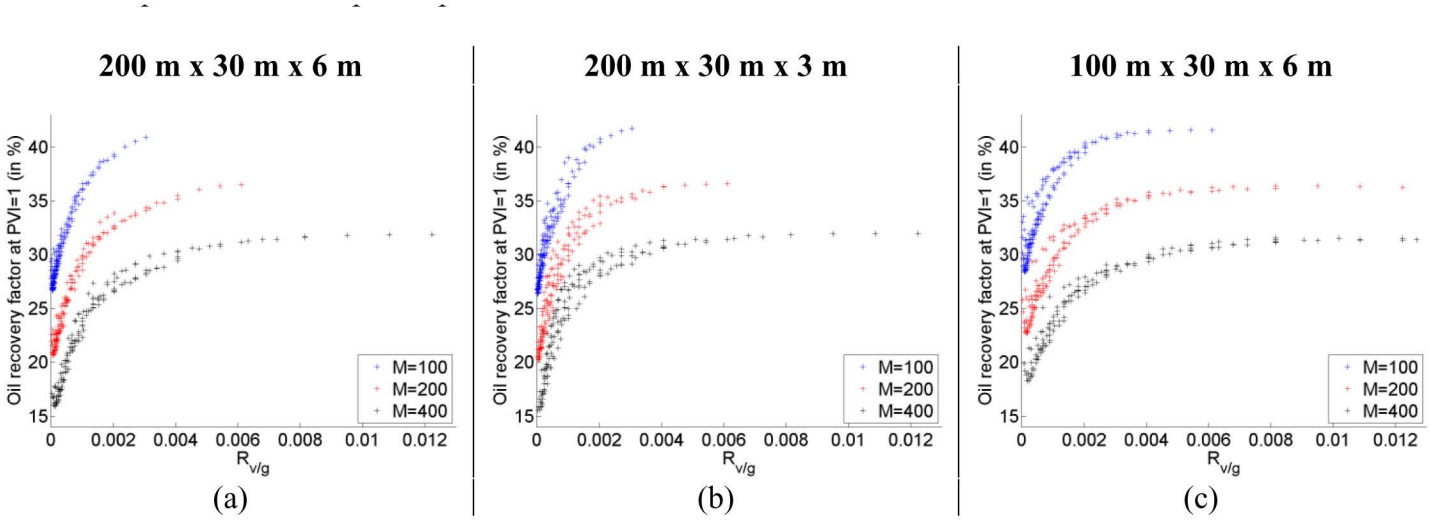

Figure 32—Oil recovery factor at PVI=1 vs. viscous-to-gravity ratio for different domain dimensions, when using $p_{c,low}$: 200 m x 30 m x 6 m (a), 200 m x 30 m x 3 m (b), 100 m x 30 m x 6 m (c)

Influence of permeability heterogeneity. We compare in *Figure 33* the oil recovery factors at PVI=0.4 & PVI=1 when using a homogeneous permeability field or heterogeneous fields with different horizontal correlation lengths (2, 5 & 10 m). Here different values of injection flow rate (4.5, 9 and 18 m³/day), fluid density difference (50, 100 and 200 kg/m³) and viscosity ratio (100, 200 and 400) were used, while setting the reservoir domain dimensions to 200 m x 30 m x 6 m, the k_v/k_h to 0.3 and the capillary pressure curve to $p_{c,low}$. The water saturation maps of the medium case at each PVI for the four different permeability fields are shown in *Figure 34*.

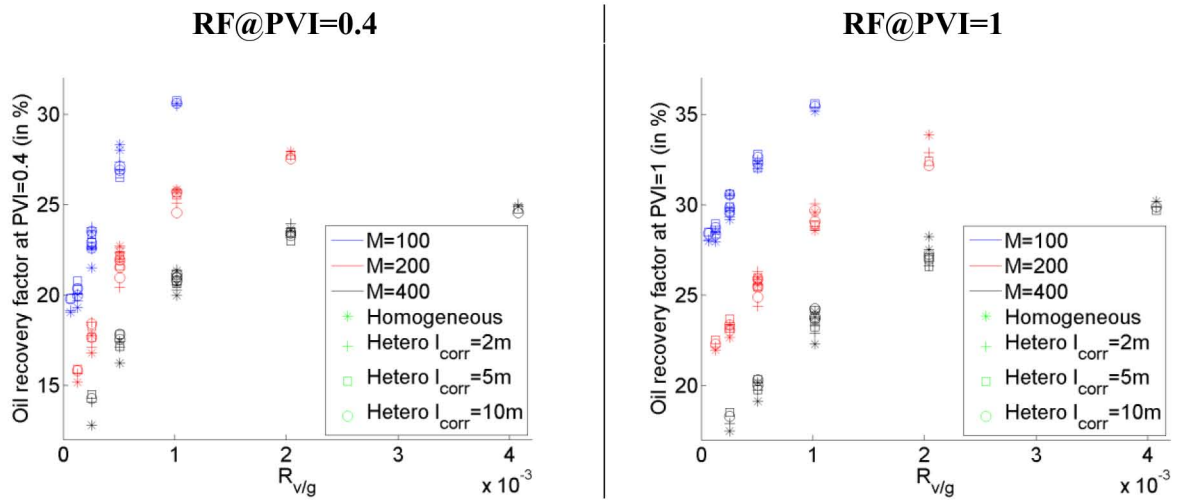

Figure 33—Oil recovery factor vs. viscous-to-gravity ratio for different viscosity ratios and permeability fields, at PVI=0.4 and PVI=1

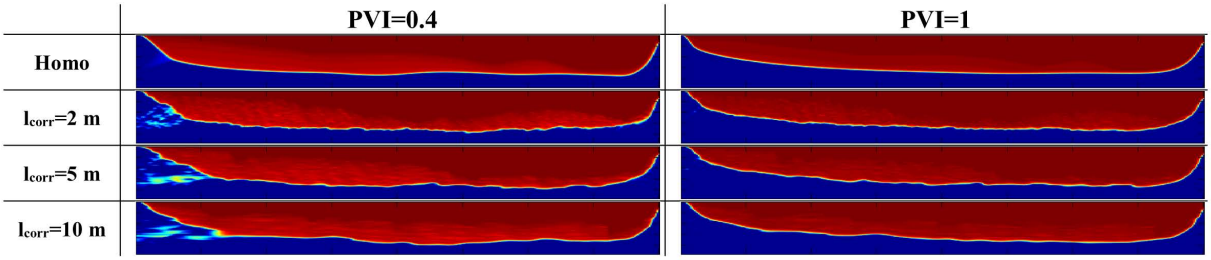

Figure 34—Water saturation maps at PVI=0.4 and PVI=1 for different permeability fields, with Q=9 m³/day, M=200 and Δρ=100 kg/m³

For all the heterogeneous permeability fields, the oil recovery remains close to that of the homogeneous field, with an absolute difference of less than 2 pp at each PVI. Indeed at late times, the flow pattern is dominated by the gravity tongue, which is only slightly impacted by the permeability field (cf. *Figure 34*).

Dependence of the oil recovery after breakthrough on $R_{v/g}$ and M for high capillary effects

We now study how the oil recovery after breakthrough depends on $R_{v/g}$ and M, when using the capillary pressure curve $p_{c,high}$. A total of 243 two-dimensional simulations were run by varying the injection flow rate (4.5, 9 and 18 m³/day), the fluid density difference (50, 100 and 200 kg/m³), the viscosity ratio (100, 200 and 400), the vertical-to-horizontal permeability ratio (0.1, 0.3 and 0.9) and the reservoir dimensions (same values as previously). For this sensitivity study, the homogeneous permeability field was used.

The RF@PVI=0.4 and RF@PVI=1 are shown in *Figure 35*: the dependence upon $R_{v/g}$ and M is not even verified at PVI=0.4, mainly due to the strong capillary effects. Indeed for a given PVI, a higher injection flow rate reduces the time period during which the spontaneous imbibition may act to improve the sweep efficiency. This is illustrated in *Figure 36* where the water saturation maps at PVI=0.4 & PVI=1 are plotted for two cases with identical ($R_{v/g}$, M), but different injection flow rates.

When capillary effects are strong, the oil recovery factor after breakthrough cannot be estimated, even roughly, using only the dimensionless numbers $R_{v/g}$ and M, as the capillary number needs to be introduced.

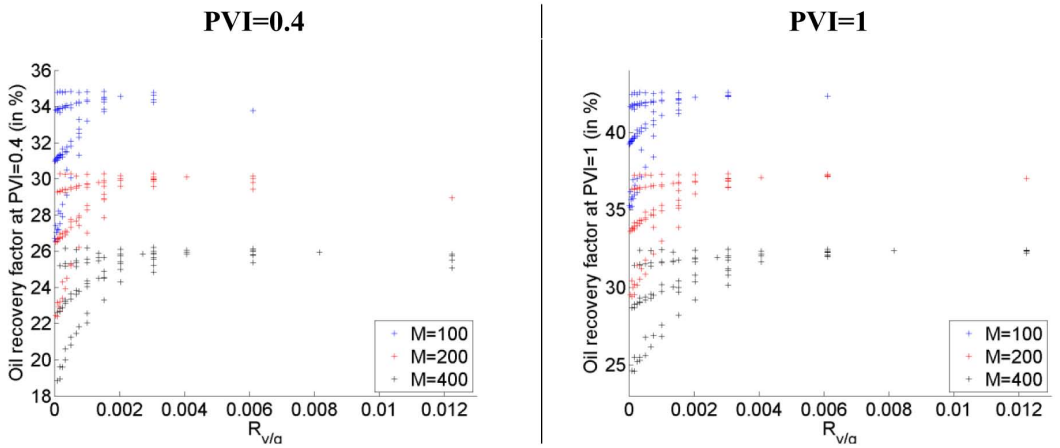

Figure 35—Oil recovery factor vs. viscous-to-gravity ratio for different viscosity ratios, when using $p_{c,high}$, at PVI=0.4 and 1

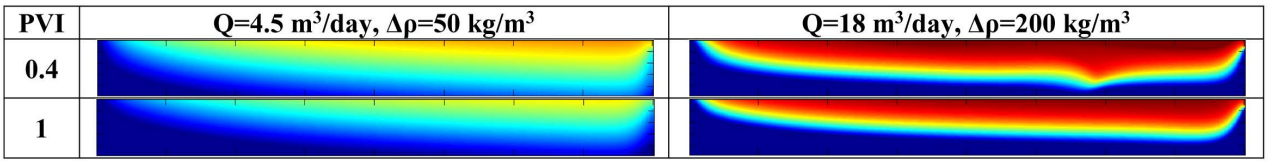

Figure 36—Water saturation maps at PVI=0.4 & PVI=1 for two cases sharing the same set of parameters ($R_{v/g}$,M), M=200, k_v/k_h=0.3, 200 m x 30 m x 6 m but with Q=4.5 m³/day & Δρ=50 kg/m³ (left) and Q=18 m³/day & Δρ=200 kg/m³ (right)

Conclusions

In this paper, the interactions between viscous and gravity effects during viscously unstable water flooding were analyzed, based on high-resolution numerical simulations of homogeneous and heterogeneous sector models representative of a viscous oil reservoir. Sensitivity studies were performed on a large set of parameters, including injection flow rate, domain aspect ratio, oil viscosity, fluid density difference and permeability anisotropy ratio.

First we identified the main flow patterns before water breakthrough: from the gravity-dominant flow regime, as the viscous effects increase, the gravity tongue gets more and more disturbed, resulting in some ridge instabilities; a transition regime then occurs, where the gravity tongue and the main viscous fingers reach the producer almost simultaneously, leading to an optimum in the oil recovery at breakthrough; finally, the viscous-dominant flow regime arises, where viscous fingering becomes more severe thus lowering the breakthrough sweep efficiency.

Next we quantified the impact of viscous instabilities in 3D domains versus 2D vertical cross-sections. We showed that 2D simulations cannot be used to accurately reproduce the early-time results, i.e. before water breakthrough. This is not only due to transverse viscous fingering – yet with a limited impact compared to the miscible case, but also to the development of ridge instabilities in the gravity tongue being sometimes impacted by 3D effects; moreover preferential paths resulting from the permeability heterogeneities cannot be captured in 2D. Nonetheless, 2D simulations are sufficient to properly replicate the 3D production results during the fully-developed regime.

We also determined that the viscous-to-gravity ratio $R_{v/g}$ along with the viscosity ratio M are not relevant enough to accurately predict the water breakthrough time (expressed in PVI), or equivalently the oil recovery at breakthrough. We thus performed detailed sensitivity studies on the main physical and geological parameters, which clarified the impact of each parameter but also revealed the complex interplay of gravity segregation, viscous fingering and permeability heterogeneity.

The two dimensionless numbers $R_{v/g}$ and M may however be used to roughly estimate the oil recovery factor after breakthrough, at least for simple heterogeneous permeability fields, but only when the capillary

effects are negligible. This may be useful to create screening models for quick-look estimation of oil recovery on different sector models representative of an oil field.

References

1. H. Tchelepi and F. Orr, "Interaction of viscous fingering, permeability heterogeneity and gravity segregation in three dimensions," *SPE Reservoir Engineering*, vol. **9**, no. 04, pp. 266-271, 1994.
2. M. Ruith and E. Meiburg, "Miscible rectilinear displacements with gravity override. Part 1. Homogeneous porous medium," *J. Fluid Mech*., vol. **420**, pp. 225-257, 2000.
3. A. Riaz and E. Meiburg, "Three-dimensional miscible displacement simulations in homogeneous porous media with gravity override," *J. Fluid Mech*, vol. **494**, pp. 95-117, 2003.
4. U. Araktingi and F. Orr Jr, "Viscous Fingering, Gravity Segregation, and Reservoir Heterogeneity in Miscible Displacements in Vertical Cross Sections," *in SPE/DOE Enhanced Oil Recovery Symposium (SPE-20176*), 1990.
5. F. Fayers and A. Muggeridge, "Extensions to Dietz theory and behavior of gravity tongues in slightly tilted reservoirs," *SPE Reservoir Engineering (SPE-18438)*, vol. **5**, no. 04, pp. 487-494, 1990.
6. F. Crane, H. Kendall and G. Gardner, "Some Experiments on the Flow of Miscible Fluids of Unequal Density Through Porous Media," *SPE Journal (SPE-535)*, vol. **3**, no. 04, pp. 277-280, 1963
7. A. Riaz and H. Tchelepi, "Linear stability analysis of immiscible two-phase flow in porous media with capillary dispersion and density variation," *Physics of fluids*, vol. **16**, no. 12, 2004.
8. A. Riaz and H. Tchelepi, "Stability of two-phase vertical flow in homogeneous porous media," *Physics of fluids*, vol. **19**, no. 7, 2007.
9. Y. Méheust, G. Løvoll, K. J. Måløy and J. Schmittbuhl, "Interface scaling in a two-dimensional porous medium under combined viscous, gravity and capillary effects," *Physical Review E*, vol. **66**, no. 5, 2002.
10. A. Riaz and H. Tchelepi, "Numerical simulation of immiscible two-phase flow in porous media," *Physics of Fluids*, vol. **18**, no. 1, 2006.
11. D. Beliveau, "Waterflooding Viscous Oil Reservoirs," SPE Reservoir Evaluation& *Engineering (SPE-113132)*, vol. **12**, no. 5, pp. 689-701, 2009.
12. M.Christie, A. Muggeridge and J. Barley, "3D Simulation of Viscous Fingering and WAG Schemes," *SPE Reservoir Engineering (SPE-21238)*, vol. **8**, no. 01, pp. 19-26, 1993.
13. Cydarex, "Cydar - User Manual," 2015.
14. A. Moncorgé, L. Patacchini and R. de Loubens, "Multi-phase, multi-component simulation framework for advanced recovery mechanisms," in Abu Dhabi International Petroleum Conference and Exhibition (SPE-161615), 2012.
15. S. Jauré, A. Moncorgé and R. de Loubens, "Reservoir Simulation Prototyping Platform for High Performance Computing," in SPE Large Scale Computing and Big Data Challenges in Reservoir Simulation Conference and Exhibition (SPE-172989), 2014
16. R. de Loubens, G. Vaillant, M. Regaieg, J. Yang, A. Moncorgé, C. Fabbri and G. Darche, "Numerical Modeling of Unstable Water Floods and Tertiary Polymer Floods into Highly Viscous Oils," in SPE Reservoir Simulation Conference (SPE-182638), 2017.
17. J. Liu, M. Delshad, G. Pope and K. Sepehrnoori, "Application of Higher-Order Flux-Limited Methods in Compositional Simulations," *Transport in Porous Media*, vol. **16**, no. 1, pp. 1-29, 1994.